PHYSICAL REVIEW B **84**, 024507 (2011)

Gap in KFe_2As_2 studied by small-angle neutron scattering observations of the magnetic vortex lattice

H. Kawano-Furukawa,[1] C. J. Bowell,[2] J. S. White,[3] R. W. Heslop,[4] A. S. Cameron,[4] E. M. Forgan,[4] K. Kihou,[5,6] C. H. Lee,[5,6] A. Iyo,[5,6] H. Eisaki,[5,6] T. Saito,[7] H. Fukazawa,[6,7] Y. Kohori,[6,7] R. Cubitt,[8] C. D. Dewhurst,[8] J. L. Gavilano,[3] and M. Zolliker[9]

[1]*Division of Natural/Applied Science, Graduate School of Humanities and Science, Ochanomizu University, Bunkyo-ku, Tokyo 112-8610, Japan*

[2]*Department of Materials Science and Metallurgy, University of Cambridge, Cambridge CB2 3QZ, United Kingdom*

[3]*Laboratory for Neutron Scattering, Eidgenössische Technische Hochschule Zurich and Paul Scherrer Institut, CH-5232 Villigen PSI, Switzerland*

[4]*School of Physics and Astronomy, University of Birmingham, Birmingham B15 2TT, United Kingdom*

[5]*National Institute of Advanced Industrial Science and Technology (AIST), Tsukuba, Ibaraki 305-8568, Japan*

[6]*Japan Science and Technology Agency, Transformative Research-Project on Iron Pnictides (TRIP), Chiyoda, Tokyo 102-0075, Japan*

[7]*Department of Physics, Chiba University, Chiba 263-8522, Japan*

[8]*Institut Laue-Langevin, 6 rue Jules Horowitz, 38042 Grenoble, France*

[9]*Laboratory for Developments and Methods, Paul Scherrer Institute, CH-5232 Villigen PSI, Switzerland*

(Received 5 May 2011; published 7 July 2011)

By neutron scattering, we have observed a well-ordered magnetic vortex lattice (VL) in KFe_2As_2 single crystals. With the field along the c axis, a nearly isotropic hexagonal VL is formed, with no symmetry transitions up to high fields, indicating a small anisotropy of the superconducting state around this axis. This rules out line nodes parallel to the c axis, and thus d-wave or anisotropic s-wave pairing. However, the strong temperature dependence of the signal at $T \ll T_c$ shows that extremely small gap values exist; these may arise from nodal lines perpendicular to the c axis.

DOI: 10.1103/PhysRevB.84.024507 PACS number(s): 74.25.Uv, 74.20.Rp, 74.70.Xa

I. INTRODUCTION

Understanding the mechanism and symmetry of electron pairing in iron-based superconductors represents an important challenge in condensed matter physics. Many theorists have suggested that high temperature superconductivity in these materials may be due to a magnetic interaction.[1] It is proposed that in optimally doped materials, there is a repulsive interaction between holes on Fermi surface (FS) sheets at the center of the Brillouin zone and the almost equal number of electrons on other sheets at the corners. The simplest form of pairing that could arise from this interaction has the opposite sign of the order parameter for the two types of carrier. Such a pairing state may be described as extended s-wave or $s_\pm$ since the order parameter has the same symmetry as the crystal and is nonzero on all parts of the FS, despite changing sign. In this respect it may be contrasted with d-wave pairing in cuprate materials, in which the order parameter has a lower symmetry than the underlying crystal, changes sign around a single sheet of FS, and therefore has nodes. Other pairing states have been proposed for the pnictides,[2,3] which maintain $s_\pm$ symmetry, but in which the order parameter also changes sign on at least one FS sheet. Our material, KFe_2As_2, belongs to the 122 family of iron pnictide superconductors; the optimally doped $BaFe_2(As_{1-x}P_x)_2$ member shows clear indications of nodes in the order parameter,[4,5] which may imply either nodal $s_\pm$ pairing or alternatively d-wave gap symmetry.[3] On the other hand, in optimally doped $Ba_{1-x}K_xFe_2As_2$ with $T_c >$ 35 K, the order parameter appears to be nodeless on all parts of the FS, although with large and small gaps on different FS sheets.[6,7] Optimally doped $BaFe_{2-x}Co_xAs_2$ is similarly nodeless.[8] Such observations raise the question whether all the iron-based superconductors, even within the 122 family, have the same gap symmetry and pairing mechanism. We note, however that nodal gaps may be observed in clean materials with long mean free paths as indicated by the observation of de Haas-van Alphen (dHvA) signals from some major portions of the Fermi surface.[9,10] Conversely, nodeless gaps may be observed in dirtier materials.[6–8] This indicates that low-energy states due to electron scattering are not a major cause of nodal behavior. It is of importance in this context to note that isovalent anion doping in the As/P material can give a long mean free path but heterovalent doping on the Fe site does not.

The vortex state in superconductors reflects the electron pairing state. However, small-angle neutron scattering (SANS) and decoration experiments before now on pnictide superconductors have shown disordered vortex lattices (VLs).[11–14] It is likely that nanoscale compositional inhomogeneity is a major source of vortex pinning and disorder in doped crystals. In KFe_2As_2, with Ba fully replaced by K, we have an overdoped but clean 122 material. Here we show how SANS measurements on the VL in this material can make a contribution to the debate on the gap structure in pnictide superconductors.

The rest of the paper is organized as follows. The next section briefly describes the sample preparation and characterization and experimental procedure. The experimental results are described and analyzed in Sec. III (details of the methods of analysis are given in the Appendices). A discussion and conclusions are in Sec. IV.

II. EXPERIMENTS

A. Sample preparation and characterization

Single crystals of KFe_2As_2 were grown in a potassium flux. The FeAs precursor was prepared from Fe and As at

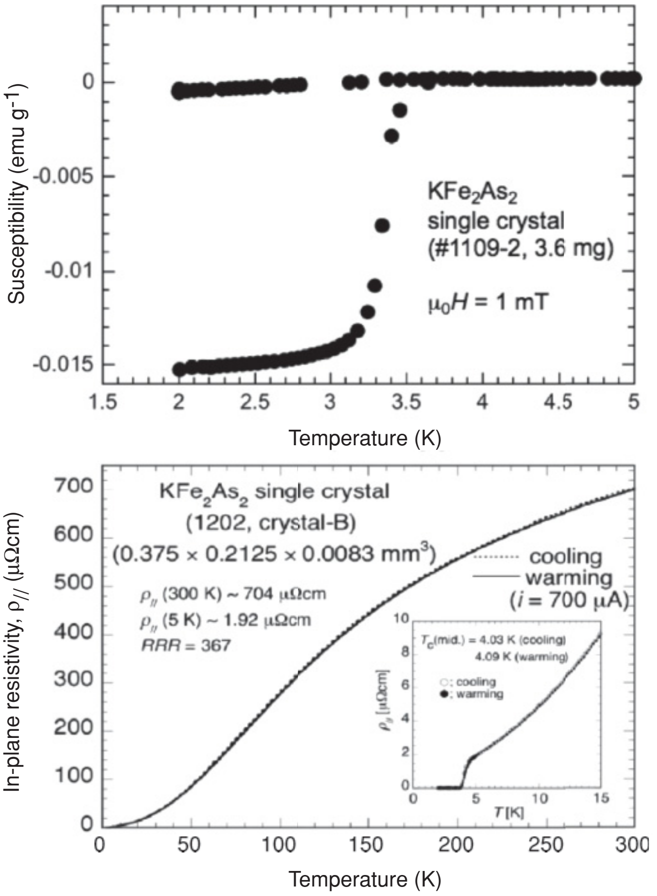

FIG. 1. Sample characterization measurements. The magnetization data were taken in an applied field of $\mu_0 H = 1$ mT; the upper curve was taken on cooling and the lower curve on heating after zero-field cooling.

900 °C for 10 h in an evacuated atmosphere and then mixed with K and As in the atomic ratio K:As:FeAs = 3:2:2. The mixture was then placed in an Al_2O_3 crucible and sealed in a stainless steel tube. The tube was heated to 900 °C, maintained at that temperature for 10 h, and cooled to 650 °C at a rate of -1 K/h, followed by quenching. The typical size of the single crystals obtained is about $7 \times 7 \times 0.5$ mm^3. To check the sample quality, we performed magnetization and resistivity measurements and results are shown in Fig. 1. Magnetization data show that T_c is 3.6 K with a 10–90 % width of 0.2 K and resistivity data give a typical residual resistance ratio ~400. Note that the field cooled (FC) and zero-field cooled (ZFC) data in the magnetization plot show large hysteresis, indicating that noticeable pinning exists at low applied field. However, we point out that the surfaces of KFe_2As_2 crystals are somewhat air sensitive, and measurements by both resistivity and superconducting quantum interference device (SQUID) techniques can be affected by surface quality. Nevertheless, dHvA (and SANS) measurements are bulk properties and show the intrinsic properties of the crystals. In addition, the upper critical field, $B_{c2}(T)$, was determined down to 1.8 K from the temperature dependence of magnetization data with B applied parallel to [0 0 1] [see Fig. 2(f)].

B. Experimental Procedure

A neutron passing through the mixed state of a superconductor experiences a spatial variation of magnetic field, and hence a variation of its spin potential energy, which can lead to diffraction of a neutron beam. Due to the long length scale of the VL (~1000 Å in our case, compared with a typical cold neutron wavelength of 10 Å) the diffraction occurs at small Bragg angles ~1°.

Small-angle neutron scattering experiments were performed on instruments D11 and D22 at the Institut Laue-Langevin (ILL), France and SANS-I at the Swiss Spallation Neutron Source (SINQ), Paul Scherrer Institut (PSI), Switzerland. A mosaic of coaligned crystals with the c axis and one of the tetragonal [1 0 0] axes in a horizontal plane was glued to aluminium sample plates with hydrogen-free CYTOP® varnish and cooled to a minimum of 1.5 K using a ^{4}He cryostat at D11 and to 50 mK using dilution refrigerators at D22 and SANS-I. The total mass of the crystals for the ILL experiments was about 100 mg and 250 mg at PSI. Magnetic fields were applied parallel to the crystal c axis and approximately parallel to the incident beam of neutrons of wavelength $\lambda_n = 10$ Å. A position-sensitive detector was set at 15 m (ILL) and 18 m (PSI) from the sample position to obtain a reasonable q resolution. Except when measuring the main beam intensity, the undiffracted beam was caught on a neutron-absorbent beamstop. The sample had sufficiently weak pinning at the fields we employed so that the VL could be formed by applying the field well below T_c; field-cooling through T_c was not required. Indeed, the VL perfection was slightly improved by oscillating the value of the field by ~0.01 T about its final value at base temperature, before taking measurements. To observe the VL diffraction, the sample and magnet were rocked together either vertically or horizontally by small angles about the $B \parallel$ beam direction to take the various diffraction spots through the Bragg condition. Backgrounds were taken with no VL present, either above T_c or by removing the applied field. Note that the real-space VL nearest-neighbor positions may be visualized by rotating the diffraction patterns by 90° about the field axis and adding another spot at the central main beam position. The SANS data were displayed and analyzed using the GRASP analysis package.[15] Further details of the analysis are given in Appendices B and D.

III. EXPERIMENTAL RESULTS

A. Vortex lattice patterns

Figures 2(a)– 2(d) show VL diffraction patterns with clear Bragg spots, measured at $T = 50$ mK and 1.5 K at selected magnetic fields applied parallel to the fourfold [0 0 1] crystal axis and approximately parallel to the neutron beam. The 12 spots arise from a mixture of two domain orientations of hexagonal VLs, which have nearest-neighbor vortices along the tetragonal [1 0 0] and [0 1 0] axes. These two orientations are degenerate because of the tetragonal crystal symmetry, and an equal mixture is to be expected from random nucleation in different parts of the sample. As shown in Appendix A, this interpretation may be confirmed, since one of these domains may be selected by rotating the field away from the c axis. White circles in the figures indicate the distance from the main

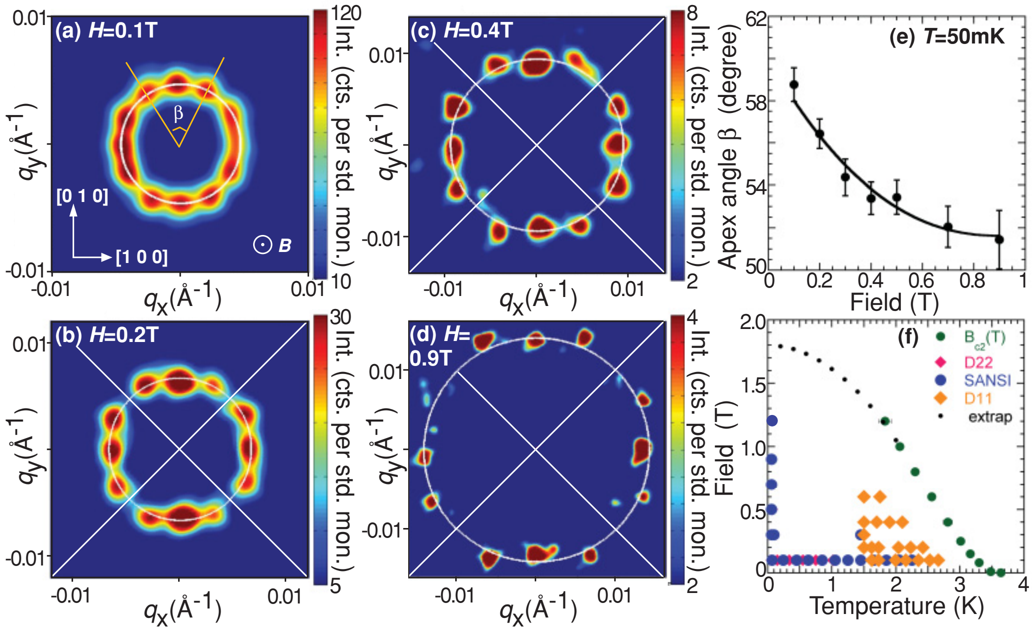

FIG. 2. (Color online) Small-angle neutron scattering patterns, VL structure, and B-T phase diagram for KFe$_2$As$_2$. (a)–(d) Diffraction patterns from the VL at (a) 0.1 T, 50 mK; (b) 0.2 T, 1.5 K; (c) 0.4 T, 1.5 K; (d) 0.9 T, 50 mK. Backgrounds obtained without VL present were subtracted. To improve visibility, the data were smoothed with a Gaussian of width comparable to the instrument resolution, and Poisson noise near the main beam was masked. The higher field patterns are mosaics of results taken at the maximum intensities of four sets of three spots, and at 0.1 T a sum over tilts is shown. (e) Field dependence of the apical angle, β, of the VL structure at $T = 50$ mK. [for definition of β see Fig. 2(a)]. (f) The B_{c2}-T phase diagram (from magnetization data with $H \parallel [0\ 0\ 1]$) indicating all conditions under which VL measurements were carried out.

beam at which regular hexagonal VL spots would appear. The offsets of the spots from the circles indicate that the VL is somewhat distorted from a pure hexagonal structure. Although the angles of the spots, which we refer as angle β, change with increasing field [Fig. 2(e)] and the observed intensity becomes weaker, the VL symmetry does not change for all conditions under which a VL signal is observed [see Fig. 2(f)].[16] In this respect, KFe$_2$As$_2$ is unlike almost all conventional and unconventional superconductors with a fourfold axis.[17–21] In conventional materials, anisotropy of the Fermi velocity leads to VL phase transitions as the field is increased.[22] This mechanism is operative in unconventional materials, too, so we conclude that the FS anisotropy is weak in KFe$_2$As$_2$. In addition, first-principles calculations using the Eilenberger theory show that gap anisotropy has similar effects,[23,24] and that a d-wave nodal gap gives rise to a square VL at a small fraction ($\sim$0.15 at $T = 0.5T_c$) of B_{c2}.[25] Experiments on d-wave materials[20,21] confirm these calculations. Since in KFe$_2$As$_2$, a square VL is absent up to 1.2 T.[26] More than half the upper critical field B_{c2} at 50 mK—we rule out a nodal order parameter with the gap varying around the c axis.

B. Field dependence of form factor

Figure 3(a) shows the B-field dependence of the VL form factor (F) derived from the integrated intensity of the on-axis VL diffraction spots at 50 mK and at 1.5 K (details are given in Appendix B). F is a measure of the spatial variation of the field inside the mixed state; it generally decreases at large field as the vortex cores begin to overlap. These data were fitted to a modified London model with core/nonlocal corrections[27]

$$F = \frac{B}{1 + q^2\lambda^2} \exp(-cq^2\xi^2) \tag{1}$$

Here, λ is the London penetration depth, ξ is the coherence length, and c is an empirical core cutoff parameter. The good fit suggests a conventional field dependence without multigap effects[28] and allows us to extrapolate to obtain the zero-field

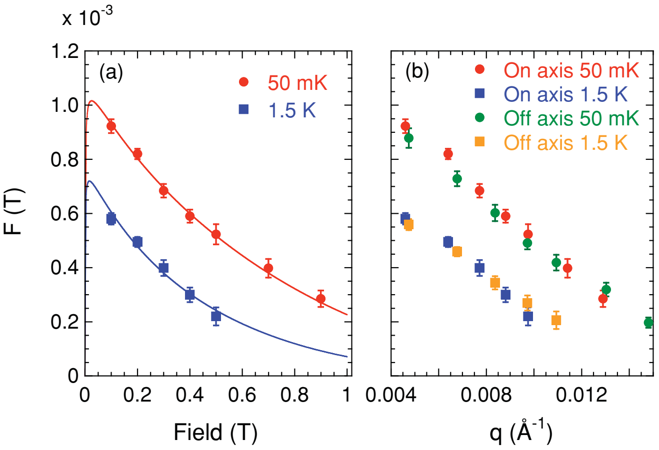

FIG. 3. (Color online) (a) Field dependence of the form factor (F) of the on-axis VL diffraction spots at $T = 50$ mK and 1.5 K. The theoretical fit is described in the text. (b) F for on- and off-axis spots at 50 mK and 1.5 K (plotted versus q values, which are different for the two types of spot).

value of λ. The best fit at 50 mK gave $\lambda = 203$ nm and $c = 0.52$, using $\xi = 13.5$ nm (from $B_{c2} = 1.8$ T), and at 1.5 K: $\lambda = 240$ nm and $c = 0.55$, with $\xi = 15.9$ nm (from $B_{c2} = 1.3$ T). Random errors in λ were small compared with probable systematic (calibration) errors $\sim$5%. The $T = 0$ value of λ may be combined with normal state properties of KFe_2As_2 (see Appendix C) to confirm a strongly enhanced carrier mass and that our samples are clean (i.e., the electron mean free path, $\ell \gg \xi_0$, the coherence length). Furthermore, in Fig. 3(b), F for both on- and off-axis spots is plotted, but against q, rather than field because the VL distortion gives the off-axis spots a larger q than the on-axis spots. We see that all results lie on nearly the same line, confirming the essential basal-plane isotropy of the pairing.

C. Temperature dependence of form factor

Measurements of the intensity I of the flux lattice diffraction signal at low fields give the magnetic penetration depth. (The $B \ll B_{c2}$ limit of Eq. (1) gives I ($\propto |F|^2$) $\propto \lambda^{-4}$ for fixed VL structure.) The temperature dependence of the penetration depth (or equivalently superfluid density) is a direct measure of the thermal excitation of quasiparticles over the gap.[29] Figure 4(a) shows the temperature dependence of the peak intensity at our lowest field of $B = 0.1$ T. The sample tilt was fixed at a value maximizing the diffracted intensity in the top spots, and data were taken versus either increasing or decreasing temperature. The constancy of the rocking curve width in the low-temperature region was checked at the arrowed temperatures. The results from SANS-I were the most complete; the data taken at other instruments were included after scaling in the overlapping regions (see Appendix D for more details). It is clear that all temperature dependencies are in agreement within statistical errors in all cases, indicating that the system is in the thermal equilibrium state and the vortices are not relaxing to a new state on temperature cycling.

Figures 4(b)–4(d) show fits of these data using the superfluid density given by sinusoidally varying nodal gaps or $\boldsymbol{k}$-independent gaps,[29] with $T = 0$ values and weights w_i given in the insets. (Full details of the fitting functions are given in Appendix D.) From Fig. 4(b), it is clear that a single nodeless gap cannot fit the low-temperature behavior; also a simple nodal gap, ignoring nonlocal effects[30] deviates from the data. However, a single nodal gap including these effects [Fig. 4(c)] can reproduce the data very well, with only one additional fitting parameter. Here nonlocal effects cause a crossover from T-linear to T^2 behavior below a temperature $T^{\star}$[30]. Similar effects can occur due to impurity scattering,[31] but are not expected to be strong in our clean material.

Alternatively, we can obtain a good fit if at least three nodeless gaps, which requires six parameters, of very different magnitudes are included, as shown in Fig. 4(d). Although this fit uses an overlarge number of parameters, we cannot rule it out, because KFe_2As_2 has multiple FS sheets,[10,32,33] which might support multivalued nodeless gaps. In all these fits, the temperature dependence of the gaps is taken as BCS-like for simplicity but the low-temperature behavior is dominated by the smallest value of the gap present at $T = 0$. The strong temperature dependence of the intensity of our diffraction signal, continuing down to at least $T \sim 0.02$ T_c, indicates that KFe_2As_2 has a range of gaps extending down to very low values. We expect that the gap is nodal, which is also suggested by recent penetration depth[33] and other measurements[34,35] performed down to various fractions of T_c.

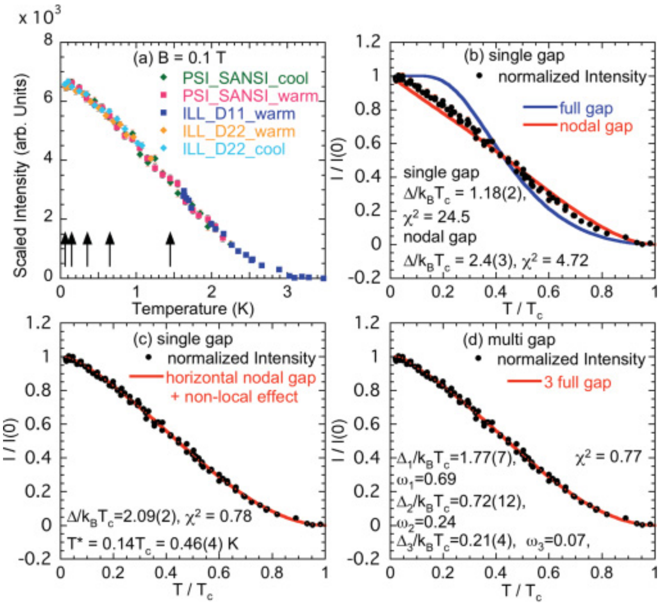

FIG. 4. (Color online) (a) Temperature dependence of peak intensity at $B = 0.1$ T. (b)–(d) Fits of the data to various gap functions versus T/T_c, with T_c set to the value $T_{c2}(0.1\ \mathrm{T}) = 3.25$ K. The fitted parameters are shown inset in the graphs: (b) single nodeless and nodal gap; (c) single nodal gap including nonlocal effects; (d) multigap model.

IV. DISCUSSION AND CONCLUSIONS

A. Gap Values

We now consider the fitted ratios $\Delta(T = 0)/k_B T_c$. The *largest* gap in a material may give a larger ratio than the weak-coupling isotropic BCS value of 1.76, either because of gap anisotropy or strong coupling. However, the largest gap cannot give a smaller ratio. This confirms that the single nodeless gap in Fig. 4(b) can be ruled out. Even in Fig. 4(d) the maximum gap is closer to the BCS limit than expected, since the other gap values are well below the limit. This argues against multiple nodeless gaps. In contrast, the fitted values of the nodal gaps in Figs. 3(b) and 3(c) have amplitudes close to the weak-coupling BCS ratio (2.14) for a sinusoidally varying order parameter. We conclude that unlike the optimally doped compositions, KFe_2As_2 is a fairly weakly coupled superconductor.

B. Gap Structure

Finally we discuss the gap structure, bearing in mind that the temperature dependence of the signal argues for a nodal state, but the VL structure measurements rule out vertical line nodes in the gap. An axially isotropic nodal pairing state would satisfy both these constraints. In this model, illustrated schematically in Fig. 5, the nodes circulate around the approximately cylindrical sheets of the FS, with the order parameter changing sign as a function of k_z, but not in the k_x-k_y plane.

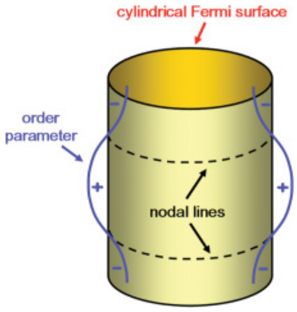

FIG. 5. (Color online) A sketch of the k_z dependence for the order parameter with a horizontal nodal gap.

For such a state, the pairing interaction should be operative in the z direction, which requires some three-dimensionality in the electronic structure; dHvA measurements[10] and the moderate anisotropy of H_{c2}[36] show that some of the FS sheets in KFe$_2$As$_2$ have a three-dimensional character. We note that T_c in (Ba/K)Fe$_2$As$_2$ appears to decrease continuously and monotonically as the doping is increased above optimal.[37] This strongly suggests that the symmetry of the order parameter does not change with doping, even though the electron sheets in optimally doped materials are replaced by small hole pockets in KFe$_2$As$_2$.[10,32,33] Our model can account for this if the in-plane pairing interaction in (Ba/K)Fe$_2$As$_2$ becomes weaker as doping is increased beyond optimal, and a nodeless gap changes into a k_z-dependent nodal gap. These two states have the same $s_\pm$ symmetry, and the node positions are accidental (not symmetry determined)[38] so the system may go continuously from one to the other as doping or carrier scattering are varied. Independently of these intriguing suggestions, we emphasize that our results rule out strongly anisotropic (e.g., d-wave) pairing in this material, but also demand that there exist Fermi surface regions with a very small gap. We also show that our sample is clean (the electron mean free path, $\ell \gg \xi_0$, the coherence length) and that the low-temperature values of ξ and λ may be understood in terms of the expected Fermi surface properties of this weakly coupled superconductor with enhanced carrier mass.

ACKNOWLEDGMENTS

We acknowledge informative discussions with A. Carrington, I. Mazin, K. Machida, and A. Maisuradze. H.K-F. was supported by the Yamada Science Foundation and Grant-in-Aid for Scientific Research on Innovative Areas (Heavy Electrons) (Grant No. 20102006) of the Ministry of Education, Culture, Sports, Science, and Technology (MEXT), Japan. C.L. was also supported by Grant-in-Aid for Scientific Research on Innovative Areas Heavy Electrons (Grant No. 20102005). H.F. and Y.K. also acknowledge support from MEXT and the Global Center of Excellence program of Chiba University. R.H., A.C., and E.F. acknowledge financial support from the United Kingdom Engineering and Physical Sciences Research Council. J.W. acknowledges financial support from the Swiss National Centre of Competence in Research program (MaNEP). We are grateful for support and allocated beam time on D11 and D22 at the Institut Laue-Langevin, Grenoble, France and on SANS-I at the spallation neutron source SINQ, Paul Scherrer Institut, Villigen, Switzerland.

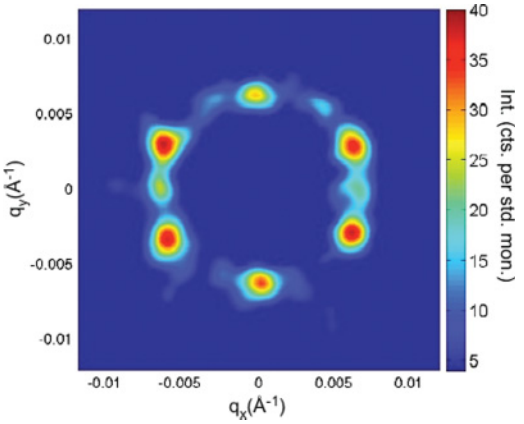

FIG. 6. (Color online) VL domain selection by altering the applied field direction.

APPENDIX A: SELECTION OF ONE VORTEX LATTICE DOMAIN ORIENTATION

Figure 6 shows the VL pattern observed at $T = 1.5$ K and $B = 0.2$ T with the sample rotated about the vertical axis so that the magnetic field is applied 10° away from the c axis toward the [1 0 0] direction [which corresponds to the horizontal axis in Figs. 2(a)– 2(d) of the main text]. Essentially a single VL domain is formed which has nearest-neighbor vortices along the [1 0 0] direction. This result confirms our interpretation of the 12-spot pattern, and shows that the field rotation removes the degeneracy between the two VL orientations. Similar effects have been observed in low-pinning crystals of niobium.[39]

APPENDIX B: METHOD TO OBTAIN FIELD DEPENDENCE OF FORM FACTOR

The local field in the mixed state may be expressed as a sum over its spatial Fourier components at the various different wave vectors q belonging to the two-dimensional reciprocal lattice of the VL. The form factor at wave vector q is the magnitude of the Fourier component $F(q)$, and the value of the form factor is obtained from the integrated intensity of a Bragg reflection as the VL is rotated through the diffraction condition. The integrated intensity, I_q is related to the modulus squared of the form factor, $|F(q)|^2$, by[40]

$$I_q = 2\pi V\phi\left(\frac{\gamma}{4}\right)^2 \frac{\lambda_n{}^2}{\Phi_0{}^2 q}|F(q)|^2. \tag{B1}$$

Here, V is the illuminated sample volume, ϕ is the incident neutron flux density, λ_n is the neutron wavelength, γ is the magnetic moment of the neutron in nuclear magnetons ($= 1.91$), and $\Phi_0 = h/2e$ is the flux quantum.

The form factors for Fig. 3(a) of the main text were determined using the on-axis (top and bottom) spots of the flux line lattice (FLL) diffraction pattern. The integrated intensity of these spots was obtained from an up-down rocking curve. Typical results are shown in Fig. 7.

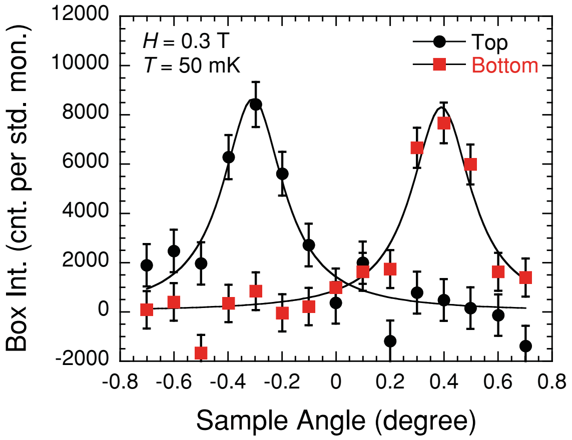

FIG. 7. (Color online) A typical example of rocking curves, taken at $H = 0.3$ T and $T = 50$ mK.

The figure shows the total counts per standard beam monitor within a box of suitable area on the detector, versus rocking angle. Annular sector-shaped boxes for these spots were chosen to capture the total intensity for the low-field data, while not being so large as to increase the Poisson error unnecessarily. The areas of the boxes (in pixels $\equiv$ solid angle) were kept approximately field independent for larger values of B. In different experiments, both angle-dependent and angle-independent backgrounds were observed. Where appropriate, backgrounds were averaged over the rocking curve, to reduce the Poisson error in the subtraction. The integrated intensity was fitted using a Lorentzian function of rocking angle, as this function minimized χ^2 at low values of field. The rocking curve width fell slightly with increasing field at low fields, and then remained constant. The statistical accuracy of the data at the highest two fields was sufficiently low that the fitted widths were not well-determined. We therefore obtained the integrated intensities at high fields by fitting the rocking curves with a Lorentzian of width set at the average value obtained at intermediate fields. When the rock direction is parallel to the $\boldsymbol{q}$ vector, the integrated intensity is the area under the rocking curves; for off-axis spots, the integrated intensity is multiplied by the Lorentz factor, $\cos(\alpha)$, where α is the angle between the $\boldsymbol{q}$ vector and the rock direction.

The incident beam intensity required for Eq. (B1) was obtained from measurements of the transmitted beam and mask area. The volume of sample employed was divided by two because of the existence of equal populations of the two FLL domain orientations. The values of q were calculated from the magnetic field and known distortions of the VL plotted in Fig. 2(e) of the main text. Errors in F were calculated either from the statistical error or the spread of the two values obtained from the top and bottom spot, whichever was the larger in each case.

APPENDIX C: RELATIONSHIP TO NORMAL STATE PROPERTIES

For a clean superconductor (the electron mean free path, $\ell \gg \xi_0$, the coherence length), the value of London penetration depth, λ_L, extrapolated to zero field and temperature, is independent of the pairing state. For our experiments, with λ_L determined by supercurrents flowing in the basal plane of a fairly two-dimensional material, it may be related to the band electronic properties by

$$\frac{1}{{\lambda_L}^2} = \sum_i \frac{n_i e^2 \mu_0}{m_i^*}. \tag{C1}$$

In this equation are added the contributions of each approximately cylindrical piece of Fermi surface, containing a number density n_i of carriers of average effective mass m_i^*. ARPES measurements,[32] band structure calculations, and dHvA measurements[10] agree that all Fermi surface sheets are hole sheets. Thus, given the unit valence of K, the total hole density n must add up to 1 per formula unit of KFe_2As_2. We therefore know the value of $n = \sum_i n_i \sim 9.7 \times 10^{27} \mathrm{m}^{-3}$.

From this, the measured value of $\lambda_L \sim 2.03 \times 10^{-7}$m allows us to calculate a band-weighted average inverse effective mass.

$$\left\langle \frac{1}{m_i^*} \right\rangle = \frac{1}{n e^2 \mu_0 {\lambda_L}^2}. \tag{C2}$$

The reciprocal of this quantity has the value 1.3×10^{-29} kg, which is $\sim$14 m_e, the free electron value. This may be compared with the dHvA masses,[10] which vary from 6 to 18 m_e. These strongly enhanced carrier masses combine with a carrier density that is smaller than that of potassium metal to give the relatively long London penetration depth.

Using the following expression for the conductivity σ in the basal plane:

$$\sigma = \sum_i \frac{n_i e^2 \tau_i}{m_i^*}, \tag{C3}$$

a band-averaged impurity scattering time $\tau = \langle \tau_i \rangle$ may be calculated from a combination of σ and the penetration depth:

$$\tau = \mu_0 {\lambda_L}^2 \sigma. \tag{C4}$$

The room temperature basal-plane resistivity of KFe_2As_2 is $\rho \sim 4.8 \times 10^{-6}\ \Omega\mathrm{m}$[36]. Our crystals have residual resistance ratio $\sim$400. From this, we obtain a low-temperature value of $\tau \sim 4.3 \times 10^{-12}$ s. For a two-dimensional material, the ratio of electron mean free path to coherence length is $\sim 3.5 k T_c \div (\hbar/\tau)$. Using $T_c(B = 0) = 3.6$ K, we obtain $\langle l/\xi_0 \rangle \sim 7.1$, which shows that our initial assumption of a clean material is self-consistent. This means that the gap function is not strongly affected by impurities, and we are observing its intrinsic form. From the low-temperature value of $B_{c2} \sim 1.8$ T, we estimate $\xi_0 = 13.5$ nm and hence the mean free path $\langle l \rangle \sim 100$ nm. For a typical observed dHvA frequency of $\sim$2 kT[10], the cyclotron radius in a field of 17 T is 95 nm. We see that the sample is just clean enough for dHvA measurements at this field.

We can make further estimates of average properties (we note that weighting of an average depends on the quantity concerned; for instance, the average mass calculated from heat capacity will not in general be equal to that from penetration depth). From the total carrier density of 1 per formula unit, which is predominantly distributed in three approximately cylindrical Fermi surfaces, we estimate the average magnitude of the Fermi wave vector $\langle k_F \rangle$ to be $3.8 \times 10^9 \mathrm{m}^{-1}$. Using $\langle m^* v_F \rangle = \hbar \langle k_F \rangle$, we obtain an average Fermi velocity $\langle v_F \rangle = 3.1 \times 10^4\ \mathrm{ms}^{-1}$. Using the relationship between coherence length and $\langle v_F \rangle$ for a two-dimensional material: $\xi_0 = \hbar v_F / 2\Delta_0 = \hbar v_F / 3.52 k T_c$, we obtain $\xi_0 = 19$ nm. This is close to the value 13.5 nm estimated from B_{c2}. We therefore find that we can obtain a good overall description of the relationships between the superconducting and normal state properties, and the electronic band structure using our approximate model, which could be further refined by treating each band separately. We conclude that our $\mathrm{KFe_2As_2}$ crystals are a clean, weakly coupled, fairly two-dimensional superconductor, with strongly enhanced carrier mass, and a Ginzburg-Landau (GL) parameter $\kappa \sim \lambda_0/\xi_0 \sim 15$ when the field is parallel to the c axis.

APPENDIX D: METHODS TO OBTAIN AND ANALYZE TEMPERATURE-DEPENDENCE DATA

At low fields, the core effects on the form factor F are small, so we may approximate to the simple London equation

$$F = \frac{B}{1 + q^2\lambda^2} \approx \frac{B}{q^2\lambda^2} \propto \frac{1}{\lambda^2} \propto \rho_s, \tag{D1}$$

where ρ_s is the superfluid density. The integrated intensity I of a diffraction spot is the peak rocked-on intensity $I_{\max} \times$ the rocking curve width and is $\propto |F|^2$ [Eq. (B1)]. The rocking curve width was not found to vary with temperature, and it would have used too much beamtime to measure it at every temperature, so we measured the temperature-dependent $I_{\max}(T) \propto \rho_s^2(T)$; fitting this to theoretical models allows us to obtain information about the gap structure.

The temperature dependence of the superfluid density may be calculated in the local limit using the following equations appropriate for a two-dimensional cylindrical Fermi surface.[29]

$$\rho_{aa/bb}(T) = 1 - \frac{1}{2\pi T}\int_0^{2\pi} \begin{pmatrix} \cos^2(\phi) \\ \sin^2(\phi) \end{pmatrix} \times \int_0^\infty \cosh^{-2}\left(\frac{\sqrt{\varepsilon^2 + \Delta_k^2(T,\phi)}}{2k_B T}\right) d\phi\, d\varepsilon. \tag{D2}$$

Here, T is the reduced temperature, ϕ is the azimuthal angle about the cylindrical Fermi surface, and $\sqrt{\varepsilon^2 + \Delta_k^2(T,\phi)}$ defines the excitation energy spectrum. Due to the fourfold rotational symmetry of the crystal, $\rho_{aa}(T) = \rho_{bb}(T)$, and therefore we may write

$$\rho_s(T) = 1 - \frac{1}{4\pi T}\int_0^{2\pi}\int_0^\infty \cosh^{-2}\left(\frac{\sqrt{\varepsilon^2 + \Delta_k^2(T,\phi)}}{2k_B T}\right) d\phi\, d\varepsilon, \tag{D3}$$

for the superfluid density. The gap function is assumed separable into temperature- and momentum-dependent factors such that $\Delta_k(\phi,T) = \Delta_k(\phi)\Delta_0(T)$, where $\Delta_k(\phi)$ describes the angular dependence of the gap function, and $\Delta_0(T)$ describes the temperature dependence. For simple estimates in the weak coupling limit, $\Delta_0(T)$ is well approximated by[41]

$$\Delta_0(T) = \Delta_0(0)\tanh\left(1.78\sqrt{\left(\frac{T_c}{T} - 1\right)}\right), \tag{D4}$$

where $\Delta_0(0)$ is the zero-temperature magnitude of the gap. The gap functions considered in our analysis include $\Delta_k(\phi) = 1$, appropriate for an isotropic s-wave gap, and the vertical node function $\Delta_k(\phi) = \cos(2\phi)$, which describes the angular variation due to a d-wave pairing state. An anisotropic s-wave state with equal positive and negative gap amplitudes may also vary sinusoidally with ϕ, and would give the same $\rho_s(T)$ as a d-wave state. (For simplicity, and to reduce the number of fitting parameters, we do not consider s-wave states with unequal positive and negative amplitudes.) Finally, a horizontal node function $\Delta_k(k_z) = \Delta_0 \cos(k_z c/2)$, which describes a gap that varies along the cylindrical axis of the Fermi surface (see Fig. 5 in the main text), also gives the same $\rho_s(T)$ as d wave. Hence, the temperature dependence on its own can only signal the presence or absence of nodes. However, from our SANS VL structural data we can infer the anisotropy of the gap and hence the geometry of any nodes. Finally, we note that for any chosen form of $\Delta_k(\phi)$, the only fitting parameter for $\rho_s(T)/\rho_s(0)$ as a function of T/T_c is $\Delta_0(0)/k_B T_c$.

At low temperatures, the local London approximation $\lambda \gg \xi_0$ is expected to break down in cases where the gap function is strongly anisotropic. This arises due to the momentum dependence of the coherence length according to $\xi_0(k) \propto 1/\Delta(k)$. Therefore in regions where $\Delta(k) \to 0$ the extreme nonlocal limit $\xi_0 \gg \lambda$ is realized and nonlocal corrections cannot be neglected. For nodal gap functions, Kosztin and Leggett[30] showed that nonlocal corrections to λ will cause the approximately T-linear behavior of $\rho_s(T)$ (which would control field penetration over distances much longer than ξ_0) to cross over to a T^2 behavior below a temperature T^*. Here, $k_B T^* \sim \Delta_0/\kappa$, and κ is the GL parameter. The simplest expression for superfluid density $n_s(T)$, which captures the behavior expected from such a nonlocal effect, is

$$n_s(T) = 1 - [1 - \rho_s(T)]\left(\frac{T_c + T^*}{T_c}\right)\left(\frac{T}{T + T^*}\right), \tag{D5}$$

where $\rho_s(T)$ is as calculated above in the local approximation. When fitting the data with this function, the temperature T^* is left free to be determined by the fit. A similar behavior at low temperatures in a nodal superconductor may also result from strong impurity scattering.[31]

For fitting multiple gaps, we make use of a simple model,[42] assuming that the contributions to the superfluid density due to each gap are both separate and additive. For a two-gap model, the total superfluid density $\rho_{\mathrm{tot}}(T)$ is given by

$$\rho_{\mathrm{tot}}(T) = \omega\rho_1(T) + (1 - \omega)\rho_2(T), \tag{D6}$$

where $\rho_1(T)$ and $\rho_2(T)$ describe the superfluid densities due to $\Delta_{1,k}(\phi,T)$ and $\Delta_{2,k}(\phi,T)$, and ω is a fitted parameter that is $\leqslant 1$ and assumed T-independent. The extension for the three-gap model is

$$\rho_{\mathrm{tot}}(T) = \omega_1\rho_1(T) + \omega_2\rho_2(T) + (1 - \omega_1 - \omega_2)\rho_3(T). \tag{D7}$$

Due to the finite field of 0.1 T being employed, the observed intensity should go to zero when the upper critical field line is crossed. Hence, the value of T_c in the fits was set to $T_{c2}(B = 0.1\ \mathrm{T})$ which was 3.25 K. In Fig. 4, we also use this value of T_{c2} to calculate $\Delta_0(0)/k_B T_c$, rather than the zero-field T_c of 3.6 K. We note that the intensity near T_c is small, goes to zero quadratically, and has little effect on the fits. On the other hand, the low-temperature behavior is determined by the gap values and gives very clear indications that small gap values are present.

In addition to the models reported in the main text, we considered a combination of a nodal nonlocal gap plus a full gap, but the weight given for the latter was so small that this did not seem a suitable model.

The data fitted in Fig. 4 in the main text were obtained from three separate experiments on three instruments: initially D11 at ILL for data above 1.5 K, then on D22 at ILL below 1.2 K, and finally on SANS-I at PSI below 2.2 K, with extra sample mass added. The data have been normalized to coincide in the crossover regions; the normalization factors used are close to those expected from absolute comparisons of the intensities on the different instruments. The sample was rocked to bring the top three diffraction spots onto the peak of their rocking curve, and held in that position during a temperature scan. A few additional measurements were taken of rocking curves at selected temperatures to confirm that the rocking curve width remained constant within errors in the lower temperature region, and hence confirm the low-temperature behavior of the temperature dependence that we obtain at fixed sample angle. The data taken on D22 was acquired by heating from base temperature, followed by cooling, and on SANS-I by cooling followed by heating. The data above 1.5 K from D11 was obtained by heating only. The agreement on temperature dependence between the instruments in their regions of overlap, and between heating and cooling in the low-temperature region provide a valuable check on the reliability of our conclusions about the low-energy gap structure.

The temperature dependence of the intensity of all spots agreed within errors, and the best statistical error (as measured by the ratio: signal/Poisson error) was obtained by taking the total scattered intensity inside an annular sector of the detector containing the top five spots. This is the quantity normalized to its value at zero temperature that is plotted in Fig. 4 in the main text.

---

[1] I. I. Mazin and J. Schmalian, Physica C **469**, 614 (2009) and references therein.

[2] K. Kuroki, H. Usui, S. Onari, R. Arita, and H. Aoki, Phys. Rev. B **79**, 224511 (2009).

[3] S. Graser, T. A. Maier, P. J. Hirschfeld, and D. J. Scalapino, New J. Phys. **11**, 025016 (2009).

[4] K. Hashimoto, M. Yamashita, S. Kasahara, Y. Senshu, N. Nakata, S. Tonegawa, K. Ikada, A. Serafin, A. Carrington, T. Terashima, H. Ikeda, T. Shibauchi, and Y. Matsuda, Phys. Rev. B **81**, 220501(R) (2010).

[5] Y. Nakai, T. Iye, S. Kitagawa, K. Ishida, S. Kasahara, T. Shibauchi, Y. Matsuda, and T. Terashima, Phys. Rev. B **81**, 020503(R) (2010).

[6] D. V. Evtushinsky, D. S. Inosov, V. B. Zabolotnyy, M. S. Viazovska, R. Khasanov, A. Amato, H.-H. Klauss, H. Luetkens, Ch. Niedermayer, G. L. Sun, V. Hinkov, C. T. Lin, A. Varykhalov, A. Koitzsch, M. Knupfer, B. Büchner, A. A. Kordyuk, and S. V. Borisenko, New J. Phys. **11**, 055069 (2009).

[7] P. Popovich, A. V. Boris, O. V. Dolgov, A. A. Golubov, D. L. Sun, C. T. Lin, R. K. Kremer, and B. Keimer, Phys. Rev. Lett. **105**, 027003 (2010).

[8] M. A. Tanatar, J.-Ph. Reid, H. Shakeripour, X. G. Luo, N. Doiron-Leyraud, N. Ni, S. L. Budko, P. C. Canfield, R. Prozorov, and Louis Taillefer, Phys. Rev. Lett. **104**, 067002 (2010).

[9] H. Shishido, A. F. Bangura, A. I. Coldea, S. Tonegawa, K. Hashimoto, S. Kasahara, P. M. C. Rourke, H. Ikeda, T. Terashima, R. Settai, Y. Onuki, D. Vignolles, C. Proust, B. Vignolle, A. McCollam, Y. Matsuda, T. Shibauchi, and A. Carrington, Phys. Rev. Lett. **104**, 057008 (2010).

[10] T. Terashima, M. Kimata, N. Kurita, H. Satsukawa, A. Harada, K. Hazama, M. Imai, A. Sato, K. Kihou, C. H. Lee, H. Kito, H. Eisaki, A. Iyo, T. Saito, H. Fukazawa, Y. Kohori, H. Harima, and S. Uji, J. Phys. Soc. Jpn. **79**, 053702 (2010).

[11] M. R. Eskildsen, L. Ya. Vinnikov, T. D. Blasius, I. S. Veshchunov, T. M. Artemova, J. M. Densmore, C. D. Dewhurst, N. Ni, A. Kreyssig, S. L. Budko, P. C. Canfield, and A. I. Goldman, Phys. Rev. B **79**, 100501(R) (2009).

[12] D. S. Inosov, T. Shapoval, V. Neu, U. Wolff, J. S. White, S. Haindl, J. T. Park, D. L. Sun, C. T. Lin, E. M. Forgan, M. S. Viazovska, J. H. Kim, M. Laver, K. Nenkov, O. Khvostikova, S. Kühnemann, and V. Hinkov, Phys. Rev. B **81**, 014513 (2010).

[13] D. S. Inosov, J. S. White, D. V. Evtushinsky, I. V. Morozov, A. Cameron, U. Stockert, V. B. Zabolotnyy, T. K. Kim, A. A. Kordyuk, S. V. Borisenko, E. M. Forgan, R. Klingeler, J. T. Park, S. Wurmehl, A. N. Vasiliev, G. Behr, C. D. Dewhurst, and V. Hinkov, Phys. Rev. Lett. **104**, 187001 (2010).

[14] L. Ya. Vinnikova, T. M. Artemovaa, I. S. Veshchunova, N. D. Zhigadloc, J. Karpinskic, P. Popovichd, D. L. Sund, C. T. Lind, and A. V. Borisd, JETP Lett. **90**, 299 (2009).

[15] C. D. Dewhurst, GRASP User Manual, Technical Report No. ILL03DE01T, Institut Laue-Langevin, Grenoble (2003), available at: [http://www.ill.fr/lss/grasp]

[16] Further observations [Furukawa *et al.* (unpublished)] indicate that there continues to be no VL symmetry change up to 1.2 T at $T =$ 50 mK.

[17] M. Laver, E. M. Forgan, S. P. Brown, D. Charalambous, D. Fort, C. Bowell, S. Ramos, R. J. Lycett, D. K. Christen, J. Kohlbrecher, C. D. Dewhurst, and R. Cubitt, Phys. Rev. Lett. **96**, 167002 (2006).

[18] M. Yethiraj, D. K. Christen, D. McK. Paul, P. Miranović, and J. R. Thompson, Phys. Rev. Lett. **82**, 5112 (1999).

[19] M. R. Eskildsen, P. L. Gammel, B. P. Barber, U. Yaron, A. P. Ramirez, D. A. Huse, D. J. Bishop, C. Bolle, C. M. Lieber, S. Oxx, S. Sridhar, N. H. Andersen, K. Mortensen, and P. C. Canfield, Phys. Rev. Lett. **78**, 1968 (1997).

[20] J. S. White, V. Hinkov, R. W. Heslop, R. J. Lycett, E. M. Forgan, C. Bowell, S. Strässle, A. B. Abrahamsen, M. Laver, C. D. Dewhurst, J. Kohlbrecher, J. L. Gavilano, J. Mesot, B. Keimer, and A. Erb, Phys. Rev. Lett. **102**, 097001 (2009).

[21] A. D. Bianchi, M. Kenzelmann, L. DeBeer-Schmitt, J. S. White, E. M. Forgan, J. Mesot, M. Zolliker, J. Kohlbrecher, R. Movshovich, E. D. Bauer, J. L. Sarrao, Z. Fisk, C. Petrović, and M. R. Eskildsen, Science **319**, 177 (2008).

[22] V. G. Kogan, M. Bullock, B. Harmon, P. Miranović, and Lj. Dobrosavljević-Grujić, P. L. Gammel, and D. J. Bishop, Phys. Rev. B **55**, R8693 (1997).

[23] N. Nakai, P. Miranović, M. Ichioka, and K. Machida, Phys. Rev. Lett. **89**, 237004 (2002).

[24] K. M. Suzuki, K. Inoue, P. Miranović, M. Ichioka, and K. Machida, J. Phys. Soc. Jpn. **79**, 013702 (2010) and references therein.

[25] M. Ichioka, A. Hasegawa, and K. Machida, Phys. Rev. B **59**, 8902 (1999).

[26] We could observe a hexagonal VL up to 1.2 T, but above 0.9 T, the signal was too weak to obtain accurate values of the apical angle and intensity.

[27] Calculations for a nodal superconductor at $T. \ll T_c$ give a dependence of F on field similar to the Gaussian expression. M. Ichioka, N. Hayashi, N. Enomoto, and K. Machida, Phys. Rev. B **53**, 15316 (1996).

[28] R. Cubitt, M. R. Eskildsen, C. D. Dewhurst, J. Jun, S. M. Kazakov, and J. Karpinski, Phys. Rev. Lett. **91**, 047002 (2003).

[29] R. Prozorov and R. W. Gianetta, Supercond. Sci. Technol. **19**, R41 (2006).

[30] I. Kosztin and A. J. Leggett, Phys. Rev. Lett. **79**, 135 (1997).

[31] P. J. Hirschfeld and N. Goldenfeld, Phys. Rev. B **48**, 4219 (1993).

[32] T. Sato, K. Nakayama, Y. Sekiba, P. Richard, Y.-M. Xu, S. Souma, T. Takahashi, G. F. Chen, J. L. Luo, N. L. Wang, and H. Ding, Phys. Rev. Lett. **103**, 047002 (2009).

[33] K. Hashimoto, A. Serafin, S. Tonegawa, R. Katsumata, R. Okazaki, T. Saito, H. Fukazawa, Y. Kohori, K. Kihou, C. H. Lee, A. Iyo, H. Eisaki, H. Ikeda, Y. Matsuda, A. Carrington, and T. Shibauchi, Phys. Rev. B **82**, 014526 (2010).

[34] H. Fukazawa, Y. Yamada, K. Kondo, T. Saito, Y. Kohori, K. Kuga, Y. Matsumoto, S. Nakatsuji, H. Kito, P. M. Shirage, K. Kihou, N. Takeshita, C. H. Lee, A. Iyo, and H. Eisaki, J. Phys. Soc. Jpn. **78**, 083712 (2009).

[35] S. W. Zhang, L. Ma, Y. D. Hou, J. Zhang, T.-L. Xia, G. F. Chen, J. P. Hu, G. M. Luke, and W. Yu, Phys. Rev. B **81**, 012503 (2010).

[36] T. Terashima, M. Kimata, H. Satsukawa, A. Harada, K. Hazama, S. Uji, H. Harima, G. F. Chen, J. L. Luo, and N. L. Wang, J. Phys. Soc. Jpn. **78**, 063702 (2009).

[37] M. Rotter, M. Pangerl, M. Tegel, and D. Johrendt, Angew. Chem., Int. Ed. **47**, 7949 (2008).

[38] P. J. Hirschfeld, Physics **2**, 100 (2009).

[39] M. Laver, C. J. Bowell, E. M. Forgan, A. B. Abrahamsen, D. Fort, C. D. Dewhurst, S. Mühlbauer, D. K. Christen, J. Kohlbrecher, R. Cubitt, and S. Ramos, Phys. Rev. B **79**, 014518 (2009).

[40] D. K. Christen, F. Tasset, S. Spooner, and H. A. Mook, Phys. Rev. B **15**, 4506 (1977).

[41] F. Gross, B. S. Chandrasekhar, D. Einzel, P. J. Hirschfield, H. R. Ott, J. Beuers, Z. Fisk, and J. L. Smith, Z. Phys. B **64**, 175 (1986).

[42] A. Carrington and F. Manzano, Physica C **385**, 205 (2003).